

# Recursive Contour-Saliency Blending Network for Accurate Salient Object Detection

Yi Ke Yun Chun Wei Tan\* Takahiro Tsubono\*  
 AI Technology Lab, OPEN8 Singapore  
 {yikey, chunweit, tsubonot}@open8.com

## Abstract

Contour information plays a vital role in salient object detection. However, excessive false positives remain in predictions from existing contour-based models due to insufficient contour-saliency fusion. In this work, we designed a network for better edge quality in salient object detection. We proposed a contour-saliency blending module to exchange information between contour and saliency. We adopted recursive CNN to increase contour-saliency fusion while keeping the total trainable parameters the same. Furthermore, we designed a stage-wise feature extraction module to help the model pick up the most helpful features from previous intermediate saliency predictions. Besides, we proposed two new loss functions, namely Dual Confinement Loss and Confidence Loss, for our model to generate better boundary predictions. Evaluation results on five common benchmark datasets reveal that our model achieves competitive state-of-the-art performance. Last but not least, our model is lightweight and fast, with only 27.9 million parameters and real-time inferencing at 31 FPS.

## 1 Introduction

Salient object detection (SOD) aims to detect and segment the most attention-attractive region or object in a visual scene. Unlike eye fixation prediction (FP) [36], SOD requires obtaining the entire region with clear boundaries. Due to its essential role and wide applications in image understanding [57], image captioning [9][43], and video summarization [27], recently, various methods have been proposed in the field.

Since 2015, Convolutional Neural Networks (CNNs) [11][17] have been adopted for SOD tasks. Though algorithms like PiCANet [24], BMPM [48], and PAGRN [51] achieved significantly better results, the predicted object usually has poor boundaries. To obtain more precise boundaries, proposed by Qin *et al.*, BASNet [33] adopted a boundary refinement U-Net [34] at the end of the saliency detection network and trained their model using various losses. In [5], Chen *et al.* proposed Contour Loss (CTLoss), which was a weighted Binary Cross-Entropy (BCE) loss, to improve the boundary predictions. Alternatively, models like EGNNet [53], PoolNet [23], and ITSD [56] fused contour predictions with saliency by explicitly supervising a contour branch. With contour cues, models yielded better boundary predictions.

However, above mentioned models still hold several problems that can be further improved. First, for better performance, many studies have introduced a huge number of trainable parameters. EGNNet contains 108 million parameters, BASNet and its extended work, U2Net [32], have more than 87 and 44 million parameters, respectively (Fig. 2). The huge number of parameters not only leads to increased consumption of computational resource, but also makes the model difficult to train. Second, though object boundary is greatly improved for contour-based networks [23][53][56], predictions

\*Corresponding author

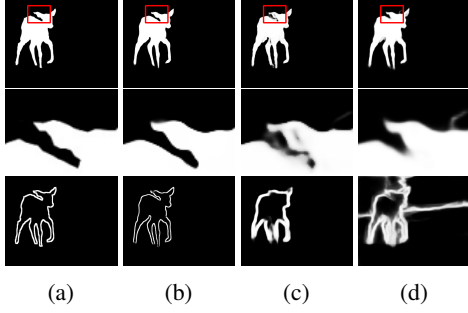


Figure 1: Visual comparisons between contour-based models. Saliency (first row) and corresponding contour predictions (last row) are listed. Ground truth contours are obtained via erosion and dilation with kernel size of 5. (a) ground truth, (b) ours, (c) ITSD [56] and (d) PoolNet [23].

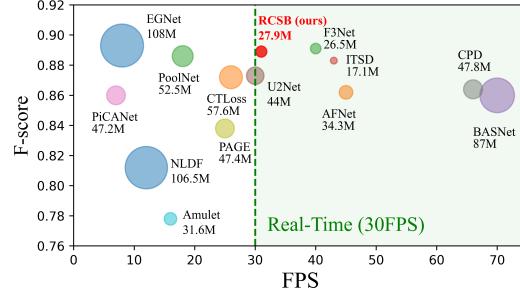


Figure 2: F-score, total parameter and FPS comparison between RCSB with 13 state-of-the-art models, including EGNet [53], PiCANet [24], C2SNet [20], PoolNet [23], PAGE [39], Amulet [50], ITSD [56], BASNet [33], U2Net [32], NLDF [25], AFNet [10], F3Net [14] and CPD [41] on DUTS-TE [37] dataset. Bubble size represents total parameters.

still have excessive false positives, as shown in Fig. 1c and 1d. Finally, to our best knowledge, for all deep learning-based models in the current field, intermediate saliency or contour predictions are generated and supervised via side branches, which introduce redundant parameters and inefficiency.

To address the abovementioned issues, we proposed a recursive contour-saliency blending network, namely, RCSBNet, for high accuracy salient object detection. We adopted a recursive CNN to reduce total trainable parameters while we can make our model deep. Unlike previous studies [23][53][56], where the contour and saliency are explicitly trained via two branches, we introduced a Contour-Saliency Blending (CSB) module in our network so that contour and saliency are intertwined and fused every step in the recursion. Meanwhile, to further improve the efficiency, we proposed a Stage-wise Feature Extraction (SFE) module to directly supervise intermediate saliency and contour predictions in the primary network without using any side branch. Lastly, we divided the training task into accuracy and confidence, and proposed Dual Confinement Loss (DCLoss) and Confidence Loss (CLoss) respectively for better model performance. To sum up, our contributions are as follows:

- (1) We proposed an efficient and accurate network, RCSBNet. By using a recursive CNN and the proposed Stage-wise Feature Extraction (SFE) module, contour and saliency are fused more efficiently and effectively.
- (2) As a favourable by-product, our model also generates contour predictions, which can be used for other computer vision tasks.
- (3) We developed two loss functions, DCLoss and CLoss, to further help the boundary prediction.
- (4) Our model has only 27.9 million parameters, which is significantly smaller than most of the networks in the field (Fig. 2).
- (5) We conducted comprehensive evaluations on 5 widely used benchmark datasets and compared with 12 state-of-the-art methods. Our method achieves competitive state-of-the-art results in all evaluation measures.

## 2 Related Work

Early approaches based on hand-crafted priors [6][13][45] have limited effectiveness and generalization ability. The very first deep salient object detection (SOD) methods [19][54] used multi-layer perceptron to predict saliency score for each image. These methods suffered from low efficiency and damage of feature structures due to flattening. Later, some studies introduced a fully convolutional network (FCN) and achieved promising results.

**Recurrent Networks.** Proposed by Kuen *et al.* [18], a recurrent network was designed to refine selected image sub-regions iteratively. In [51], Zhang *et al.* designed a multi-path recurrent model for saliency detection by transferring global information from deep layers to shallower layers. Similarly,

by iteratively correcting prediction errors, Wang *et al.* [38] developed a recurrent CNN for salient object detection. Hu *et al.* [35] proposed their salient object detection model by concatenating multi-layer deep features recurrently. It was proved that saliency predictions will be refined by using recurrent mechanism.

**Recursive Learning.** In [28], a recursive convolutional neural network (RCNN) was proposed for object detection. The main idea was to unfold the same convolution layer several times while weights are shared. It had the advantage that model depth can now be deeper by unfolding, while the total number of trainable parameters remains the same. It also revealed that, by increasing the number of recursions, better results would be obtained. Similarly, Zamir *et al.* introduced a feedback mechanism, and the corresponding feedback network [47] made predictions iteratively. Instead of simply stacking convolution layers together, recursive learning yielded better results and kept the total number of trainable parameters constant by weight sharing between layers.

**Utilizing Contour Information.** In recent years some studies explored and verified the effectiveness of involving contour information to improve the accuracy of saliency prediction. In [5], Chen *et al.* considered boundary pixels as hard samples and proposed a contour loss, which was a weighted BCE loss, to train their network. Qin *et al.* [33] combined Structural Similarity Index (SSIM), Intersection over Union (IOU), and BCE as their contour-aware loss function to achieve better boundary quality. In another seminal work, Salient Edge Detector (SED) [39] was introduced to simultaneously generate saliency and contour predictions by using a residual structure. Furthermore, PoolNet [23] applied multi-task training and fused the contour information with saliency predictions. Later, ITSD [56] proposed a two-stream network to convert saliency and contour interactively and yielded good boundary predictions. These studies further corroborated the importance of employing contour information to improve saliency predictions.

### 3 RCSBNet

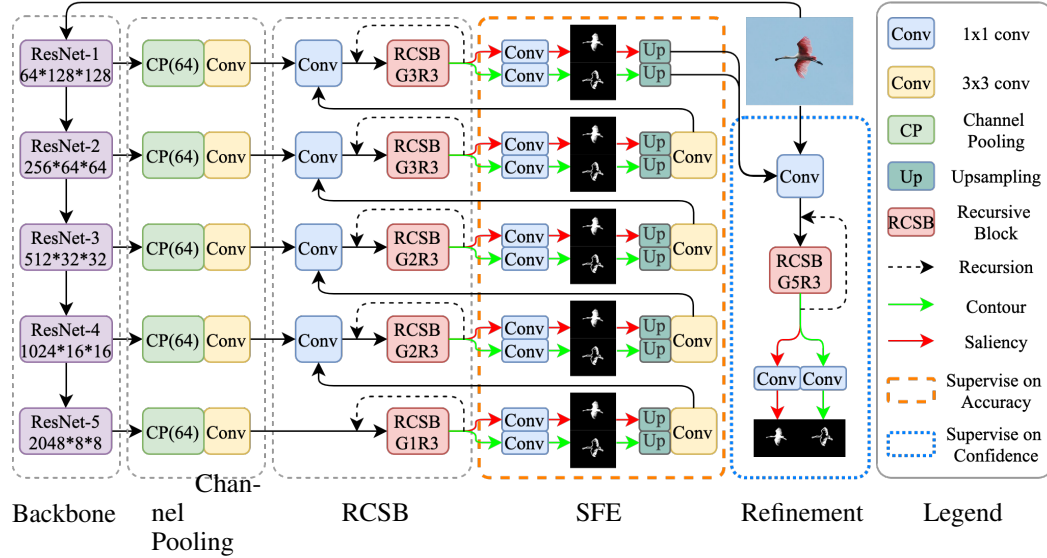


Figure 3: Network architecture for RCSBNet. Pre-trained ResNet-50 is used as the backbone, channel number is reduced to 64 via Channel Pooling (CP) layer. Recursive Contour-Saliency Blocks (RCSB) with  $G$  blocks and  $R$  recursions are then attached and followed by Stage-wise Feature Extraction (SFE) module to generate contour and saliency predictions. At the end of the network, a refinement module is adopted to further refine the predictions.

#### 3.1 Overall Architecture

In previous contour-related networks [23][53][56], either the contour was supervised in a separate branch to guide the saliency prediction, or it was fused with saliency stage by stage to achieve better

boundary predictions. Both approaches gave promising results, but there are two major disadvantages: 1) *late fusion*: contours are fused with saliency at the end of each stage. 2) *limited fusion*: the number of fusion is limited by the number of U-Net stages. For *late fusion*, we designed a Contour-Saliency Blending Unit (CSBU) so that contour and saliency information can be exchanged at a much earlier stage, while for *limited fusion*, a recursive mechanism was adopted to circumvent this constraint.

As shown in Fig. 3, the proposed RCSBNet is essentially a U-Net, where we employ pre-trained ResNet-50 as our encoder and a customized decoder adopting recursive CNNs. Contour and saliency are blended in the recursion block by the Contour-Saliency Blending Unit (CSBU). Then saliency and contour features are split and fed into the Stage-wise Feature Extraction (SFE) module for supervised learning. At the last stage of the decoder, we concatenate the prediction of contour and saliency with the input image, followed by an additional recursive block, to generate the final predictions.

### 3.2 ResNet-50 as the Encoder

We employ the pre-trained ResNet-50 as our encoder. Since it contains a large number of feature maps in high-level blocks, same as [56], we apply channel pooling (CP) to reduce the number of channels to 64, and the operation can be expressed as:

$$CP = \text{collect}_{j \in [0, m-1]} (\max_{k \in [0, \frac{n}{m}-1]} X^{j \times \frac{n}{m} + k}) \quad (1)$$

where  $j, k$  are integers, and we divide total  $n$  channels into  $m$  groups then apply max-pooling. A convolution layer is attached after the channel pooling layer to prepare the features for further processing by the decoder, as shown in Fig. 3.

### 3.3 Contour-Saliency Blending Unit (CSBU)

Contour information is usually supervised and fused with saliency at the end of each U-Net stage. For us, we want to fuse the contour and saliency at earlier stages and as many times as possible. Inspired by Shuffle-Net [52], where convolution was divided into groups and information is exchanged by shuffling the weight channels, we designed our Contour-Saliency Blending Unit (CSBU). As illustrated in Fig. 4a, the CSBU has a contour branch and saliency branch. Features generated by each branch are concatenated and blended. Mathematically, let  $F_{k \times k}^{sal}$  and  $F_{k \times k}^{ctr}$  denote the convolution for saliency and contour with kernel size  $k$  respectively, while  $(C_{n-1}, S_{n-1})$  and  $(C_n, S_n)$  represent contour and saliency features before and after CSBU. For simplicity, we omit ReLU [2] and BatchNorm [12] in our formula, and then the proposed CSBU can be modeled as:

$$CTR = F_{3 \times 3}^{ctr}(C_{n-1}), \quad SAL = F_{3 \times 3}^{sal}(S_{n-1}) \quad (2)$$

$$C_n = F_{3 \times 3}^{ctr}(F_{1 \times 1}^{ctr}([CTR, SAL])), \quad S_n = F_{3 \times 3}^{sal}(F_{1 \times 1}^{sal}([CTR, SAL])) \quad (3)$$

and thus:

$$S_n, C_n = CSBU(S_{n-1}, C_{n-1}) \quad (4)$$

By applying CSBU, contour and saliency information can be utilized by the network at a much earlier stage.

### 3.4 Recursive Block

We now introduce more details of the recursive block, as illustrated in Fig. 4b. Firstly let us consider a single recursive block then we extend to more general cases. We denote  $R$  as the total number of recursions in a single block, and  $f^r (r = 1, 2, \dots, R)$  denote the  $r^{th}$  recursion of the CSBU. Based on Eq. 4, let  $X_{n-1}$  denote the input tuple of  $(S_{n-1}, C_{n-1})$ , and  $X_R$  represent the output of the  $R^{th}$  recursion, then we have:

$$X_R = f^R(\dots(f^2(f^1(X_{n-1}) + X_{n-1}) + X_{n-1}) + \dots + X_{n-1}) \quad (5)$$

note that weights for CSBU are shared in recursion, though they have different superscripts in the formula. Then we apply a single convolution layer, denoted as  $F_{3 \times 3}$ , at the end of recursion with skip connection. Thus the output of our recursive block,  $X_n$ , is:

$$X_n = F_{3 \times 3}(X_R + X_{n-1}) + X_{n-1} = h_b(X_{n-1}) \quad (6)$$

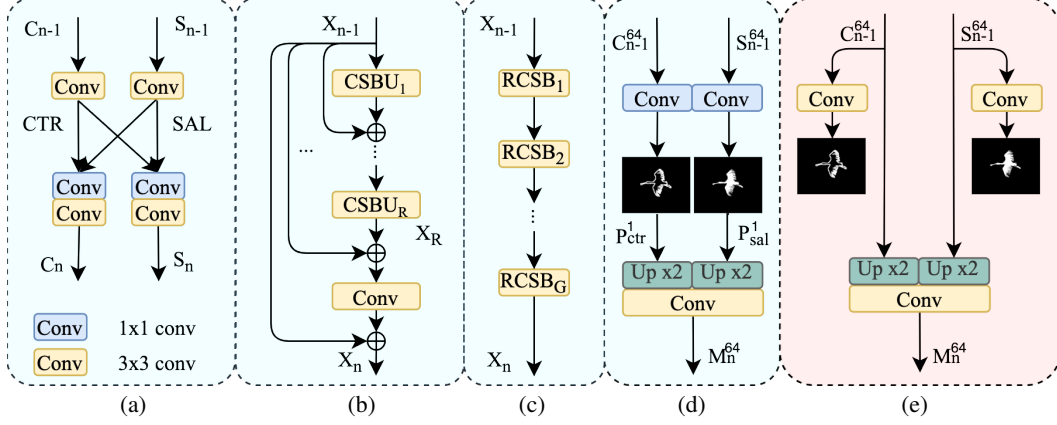


Figure 4: (a) Contour-Saliency Blending Unit (CSBU). It contains two streams where contour and saliency information are blended and intertwined. (b) Single Recursive Contour-Saliency Blending (RCSB) Block. In order to increase the number of contour-saliency fusion, recursive mechanism is applied. Weights are shared among all CSBU blocks used in the RCSB. (c) Network branch contains  $G$  blocks of RCSB, each with  $R$  times of recursion. (d) Stage-wise Feature Extraction (SFE) module. (e) Conventional methods for generating intermediate stage predictions by using side branches.

where  $h_b$  represents the recursive block function.

Now let  $G$  represent the total number of recursive blocks, as shown in Fig. 4c, in our network we simply stack all the recursive blocks together. Thus the output of  $g$ -th block,  $X_n$ , is:

$$X_n = h_b^g(h_b^{g-1}(\dots h_b^2(h_b(h_b(X_{n-1})))))) \quad (7)$$

where  $h_b^g$  represents the  $g$ -th recursive block function.

By applying recursive blocks and stacking them together, contour and saliency can now be fused  $G \times R$  times at each stage of the U-Net, which will improve the network performance significantly. We will show more results in Sec. 4.

### 3.5 Stage-wise Feature Extraction (SFE) Module

It is prevalent that saliency networks are densely supervised, where intermediate stage features are generated and supervised against ground truths to guide the model for better convergence. Common practices create a side branch with a few convolution layers to generate predictions from current U-Net stage features, following which the stage features are passed on to the next U-Net stage in the primary network (Fig. 4e). Different from others, we regard stage predictions as the best result the network can obtain so far and apply a new round of feature extraction based on current stage predictions. Therefore, stage predictions are now in the network's main branch, acting as a single channel layer, and supervised against ground truths, as illustrated in Fig. 4d. By doing so, the next block is expected to extract valuable features from current best results and discard all useless features, which might otherwise be carried along by recursion and residual connections.

To generate stage predictions, unlike previous studies [3][23][56], we do not use max-pooling because it will bring false positives to the next stage, nor the element-wise multiplication between contour and saliency like SCRN [42] due to the introduction of false negatives. Instead, we employ a  $1 \times 1$  convolution and a scaling factor to help sigmoid function classify saliency and background. To formulate the SFE module mathematically, let  $C^i$  and  $S^i$  represent incoming  $i$  channels of feature maps, and  $K$  represent the scaling factor learned by the network, then stage prediction  $P^j$  with  $j$  channels can be expressed as:

$$P_{sal}^1 = F_{1 \times 1}^{sal}(S_{n-1}^{64}) * K_{sal}, \quad P_{ctr}^1 = F_{1 \times 1}^{ctr}(C_{n-1}^{64}) * K_{ctr} \quad (8)$$

where  $*$  represents element-wise multiplication. For extracted feature maps  $M_n^j$  with  $j$  channels:

$$M_n^{64} = F_{3 \times 3}(Up^{\times 2}[\sigma(P_{sal}^1), \sigma(P_{ctr}^1)]) \quad (9)$$

where  $\square$  stands for concatenating,  $Up^{\times 2}$  is up-sampling, and  $\sigma$  stands for sigmoid function.

### 3.6 Loss Functions

Unsure prediction is very common in salient object detection in the form of shady areas (Fig. 5b). Many studies try to improve the performance by focusing on hard pixels near the boundary [5][14]. Boundary pixels are indeed hard samples, but not all the hard samples are near the boundary. We notice that the network can correctly predict the saliency for some images, but with low pixel values; while for some other images, the network is confident of generating false negatives (FN) or false positives (FP), as illustrated in Fig. 5e and 5f. It points out two kinds of difficulties encountered by the network: 1) unconfident but accurate predictions and 2) confident but inaccurate predictions. Hence in addition to accuracy, we factor in the confidence of predictions, and we introduce Confidence Loss (C Loss) to our training.

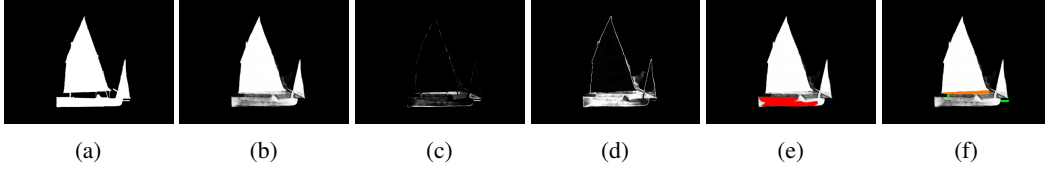


Figure 5: (a) ground truth saliency. (b) predicted saliency. (c) focal loss ( $\alpha, \gamma = 2, 2$ ) weight map calculated using (a) and (b). (d) confidence loss ( $\beta, \lambda = 2, 1$ ) weight map calculated using (a) and (b). (e) unconfident but correct area (red) in prediction. (f) confident false positives (orange) and false negatives (green) in prediction. Compare (d) with (c), focal loss is less sensitive to unsure predictions, while confidence loss generates high weights especially on object boundaries, which eventually help the model generate sharper edges.

**Confidence Loss.** Recently focal loss [22][40] has been explored in saliency tasks due to its high weight on wrong predictions:  $W_{focal} = \alpha(\hat{y}_{i,j} - x_{i,j})^\gamma$ . However, focal loss becomes less sensitive as predictions approach ground truth, which eventually leaves a large area of unsure predictions.

In order to guide the model focus more on the unconfident predictions, we propose a confidence score,  $W_c$ , for each pixel  $x_{i,j}$  in prediction:

$$W_c = \beta * x_{i,j} * (1 - x_{i,j}) \quad (10)$$

where  $\beta$  is empirically set to 2, and  $x_{i,j}$  is the prediction after sigmoid. When  $x_{i,j} = 0.5$  the score reaches its maximum. Then with ground truth  $\hat{y}_{i,j}$ , our confidence loss (C Loss),  $\mathcal{L}_{con}$ , is defined as:

$$\mathcal{L}_{con}(\beta, \lambda) = -\frac{1}{n} \sum_{i=1}^n [W_c * BCE(x_{i,j}, \hat{y}_{i,j}) + \lambda W_c] \quad (11)$$

where  $\lambda$  is set to 0.3 by parameter search. By applying this loss, it will encourage the model to make more confident predictions into either foreground (close to 1) or background (close to 0).

**Dual Confinement Loss.** In [5] and [56], a weight map generated from contour ground truth is applied to BCE loss to improve saliency boundary predictions. Based on this, we designed our Dual Confinement Loss (DCLoss), where we use weight maps generated from saliency ground truths to improve contour predictions and vice versa. This is because saliency and contour are not two explicitly separate streams but are intertwined. Losses for each stream,  $\mathcal{L}_{sal}$  and  $\mathcal{L}_{ctr}$ , are defined as:

$$\mathcal{L}_{sal} = -\frac{1}{n} \sum_{i=1}^n [W_{sal} * BCE(x_i^{sal}, \hat{y}_i^{sal})], \quad \mathcal{L}_{ctr} = -\frac{1}{n} \sum_{i=1}^n [W_{ctr} * BCE(x_i^{ctr}, \hat{y}_i^{ctr})] \quad (12)$$

where weight matrix  $W_{sal}$  and  $W_{ctr}$  are calculated by:

$$W_{sal} = \max(x_i^{ctr}, \hat{y}_i^{ctr}) * \theta + 1, \quad W_{ctr} = \max(x_i^{sal}, \hat{y}_i^{sal}) * \theta + 1 \quad (13)$$

where  $x, \hat{y}$  stand for prediction and ground truth, and empirically, we set  $\theta = 4$  in our experiments. Then the DCLoss,  $\mathcal{L}_{DC}$ , is defined as:

$$\mathcal{L}_{DC} = \mathcal{L}_{sal} + \mathcal{L}_{ctr} \quad (14)$$

**Loss for Training.** Compared with low-level predictions, it should be relatively easy to emphasize accuracy on high-level predictions due to its small feature dimension. Meanwhile, a failure in high-level predictions will impact its following decoders and eventually cause false positives or negatives.

Thus, we train stages 1 to 5 of our network against accuracy-related losses, i.e. DCLoss and weighted IOU loss mentioned in [14], and train the refinement module against CLoss only. Our loss functions for saliency and contour are defined as:

$$\mathcal{L}_{saliency} = \mathcal{L}_{DC}^{1-5} + \mathcal{L}_{wIOU}^{1-5} + \mathcal{L}_{con}^{ref}(\beta, \lambda = 2, 0.3), \quad \mathcal{L}_{contour} = \mathcal{L}_{DC}^{1-5} + \mathcal{L}_{con}^{ref}(\beta, \lambda = 2, 0.3) \quad (15)$$

where superscripts 1 – 5 and *ref* represent the five decoder stages and refinement module in Fig. 3.

## 4 Experiments

### 4.1 Datasets

We evaluate our model on five benchmark datasets, including DUT-OMRON [46] with 5168 images, ECSSD [44] with 1000 images, PASCAL-S [21] with 850 images, HKU-IS [19] with 4447 images, and DUTS-TE [37] with 5019 Images. Besides, five metrics are used to evaluate the performance between RCSB and other state-of-the-art models, which will be elaborated more in Sec. 4.3.

### 4.2 Implementation Details

To train the network, we use DUTS-TR [37] as our training dataset. During training, input images are resized to 256×256, then random horizontal flipping and 90° rotation are applied as the augmentation. We use pre-trained ResNet-50 [11] as the encoder backbone. The number of recursive blocks *G* is set to (1, 2, 2, 3, 3, 5) with recursion *R* = 3 for the decoder and refinement module (Fig. 3). Besides, Leaky ReLU [15] is applied in our implementation. We adopt the Adam optimizer [16] with default hyperparameters to train our network. Learning rates for encoder and decoder are set to  $10^{-5}$  and  $10^{-4}$  respectively, and they are halved every 20 epochs with a total of 100 epochs using batch size of 4. During testing, images are resized to 256×256, and the predictions (256×256) are resized back to their original size by using bilinear interpolation. We implement our network using PyTorch [31] and a single RTX 3090 GPU for all our experiments. For an image of size 256×256, the inference speed can reach 31 FPS, which is real-time. Code is available at: <https://github.com/BarCodeReader/RCSB-PyTorch>.

### 4.3 Evaluation Metrics

To evaluate the performance, Precision-Recall (PR) curve,  $F_\beta$ -measure [1], Mean Absolute Error (MAE),  $S_\alpha$ -measure [7], and  $E_\xi$ -measure [8] are adopted in our experiments.

**PR-Curve.** By applying different thresholds from 0 to 255, PR curve is obtained by comparing the ground truth masks against the binarized saliency predictions.

**F-measure.** The  $F_\beta$ -measure is calculated by precision and recall value of saliency maps:  $F_\beta = \frac{(1+\beta^2) \times \text{Precision} \times \text{Recall}}{\beta^2 \times \text{Precision} + \text{Recall}}$  where  $\beta^2$  is set to 0.3 [1]. We report the best score over all thresholds from 0 to 255 and denote as  $F_\beta^*$  [26][49].

**Mean Absolute Error (MAE).** MAE is the mean value of the sum of pixel-wise absolute differences between predictions  $x$  and ground truths  $\hat{y}$ :  $MAE = \frac{1}{n} \sum_{i=1}^n |x_i - \hat{y}_i|$ .

**S-measure.**  $S_\alpha$  measures the region and object level of structural similarities between the prediction and the ground truth, denoted as  $S_o$  and  $S_r$ . It is defined as  $S_\alpha = \alpha S_o + (1 - \alpha) S_r$  with  $\alpha = 0.5$ .

**E-measure.** By using local pixel values and the image-wise mean,  $E_\xi$  calculates the similarity between the prediction and the ground truth.

### 4.4 Comparisons with State-of-the-art Results

We compare our results with 12 state-of-the-art salient object detection networks, including AFNet [10], PAGE [39], CPD [41], BASNet [33], PoolNet [23], CAGNet [29], GateNet [55], ITSD [56], U2Net [32], GCPA [4], MINet [30], and F3Net [14]. All saliency maps used are provided by authors or computed by their official released code.

**Quantitative Evaluation.** To compare our work with the state-of-the-art networks, detailed experimental results in terms of four metrics are listed in Table 1. Among all the models, RCSBNet achieves



Table 1: Quantitative comparisons between RCSBNet and other 12 methods on five benchmark datasets in terms of the maximum F-measure  $F_\beta^*$ , MAE  $M$ ,  $E_\xi$  and  $S_\alpha$ .  $\uparrow/\downarrow$  means the larger/smaller the value, the better the results. **Red**, **Green**, and **Blue** indicate the best, second best and third best performance.

Method	DUTS-TE				HKU-IS				PASCAL-S				ECSSD				DUT-OMRON			
	$F_\beta^* \uparrow$	$M \downarrow$	$E_\xi \uparrow$	$S_\alpha \uparrow$	$F_\beta^* \uparrow$	$M \downarrow$	$E_\xi \uparrow$	$S_\alpha \uparrow$	$F_\beta^* \uparrow$	$M \downarrow$	$E_\xi \uparrow$	$S_\alpha \uparrow$	$F_\beta^* \uparrow$	$M \downarrow$	$E_\xi \uparrow$	$S_\alpha \uparrow$	$F_\beta^* \uparrow$	$M \downarrow$	$E_\xi \uparrow$	$S_\alpha \uparrow$
AFNet <sub>19</sub> [10]	.862	.046	.879	.867	.923	.036	.942	.905	.867	.078	.846	.844	.935	.042	.918	.913	.797	.057	.853	.826
PAGE <sub>19</sub> [39]	.838	.051	.854	.869	.930	.037	.940	.903	.835	.078	.835	.841	.931	.042	.920	.912	.791	.066	.853	.824
CPD <sub>19</sub> [41]	.865	.043	.886	.869	.925	.034	.944	.905	.864	.072	.849	.842	.939	<b>.037</b>	<b>.924</b>	.918	.797	.056	.866	.825
BASNet <sub>19</sub> [33]	.860	.047	.884	.866	.928	.032	.946	.909	.854	.076	.847	.832	.942	<b>.037</b>	<b>.921</b>	.916	.805	.056	<b>.869</b>	.836
PoolNet <sub>19</sub> [23]	<b>.886</b>	.040	.889	.883	.934	.032	<b>.949</b>	.916	.863	.075	.850	.845	.940	.042	<b>.924</b>	.921	<b>.830</b>	.055	.863	.835
CAGNet <sub>20</sub> [29]	.866	.040	.897	.864	.926	<b>.030</b>	.945	.904	.859	.066	<b>.857</b>	.835	.937	<b>.037</b>	.916	.908	.791	<b>.054</b>	.856	.815
GateNet <sub>20</sub> [55]	<b>.888</b>	.040	.889	<b>.885</b>	.933	.033	<b>.949</b>	.915	<b>.875</b>	.068	<b>.852</b>	.851	.945	.040	<b>.924</b>	.920	.818	.055	.862	.838
ITSD <sub>20</sub> [56]	.883	.041	.895	<b>.885</b>	.934	.031	<b>.952</b>	<b>.917</b>	.871	.070	.850	<b>.853</b>	<b>.947</b>	<b>.035</b>	<b>.927</b>	<b>.925</b>	<b>.823</b>	.061	.863	<b>.840</b>
U2Net <sub>20</sub> [32]	.873	.045	.886	.874	<b>.935</b>	.031	.948	.916	.862	.076	.841	.838	<b>.951</b>	<b>.033</b>	<b>.924</b>	<b>.928</b>	<b>.823</b>	<b>.054</b>	<b>.870</b>	<b>.846</b>
GCFA <sub>20</sub> [4]	<b>.888</b>	.038	.891	<b>.891</b>	<b>.938</b>	.031	<b>.949</b>	<b>.920</b>	.869	<b>.061</b>	.847	<b>.858</b>	<b>.948</b>	<b>.035</b>	.920	<b>.927</b>	.812	.056	.860	<b>.839</b>
MinNet <sub>20</sub> [30]	.884	<b>.037</b>	<b>.898</b>	.884	<b>.935</b>	<b>.029</b>	<b>.953</b>	<b>.919</b>	.867	.063	.851	.850	<b>.947</b>	<b>.033</b>	<b>.927</b>	<b>.925</b>	.810	.055	.865	.833
F3Net <sub>20</sub> [14]	<b>.891</b>	<b>.035</b>	<b>.902</b>	<b>.888</b>	<b>.937</b>	<b>.028</b>	<b>.953</b>	<b>.917</b>	<b>.872</b>	<b>.062</b>	<b>.859</b>	<b>.855</b>	.945	<b>.033</b>	<b>.927</b>	.924	.813	<b>.053</b>	<b>.870</b>	.838
Ours	<b>.888</b>	<b>.036</b>	<b>.904</b>	.878	<b>.935</b>	<b>.028</b>	<b>.949</b>	.911	<b>.873</b>	<b>.059</b>	<b>.852</b>	.846	.945	<b>.037</b>	.919	.916	<b>.820</b>	<b>.049</b>	<b>.867</b>	.832

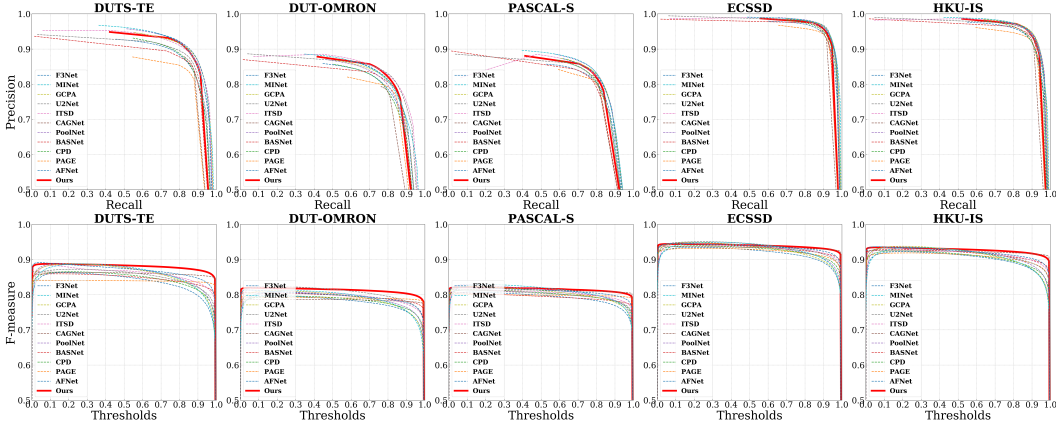


Figure 6: First row: Precision-Recall Curves comparison on five saliency benchmark datasets. Second row: F-measure Curves comparison on five saliency benchmark datasets.

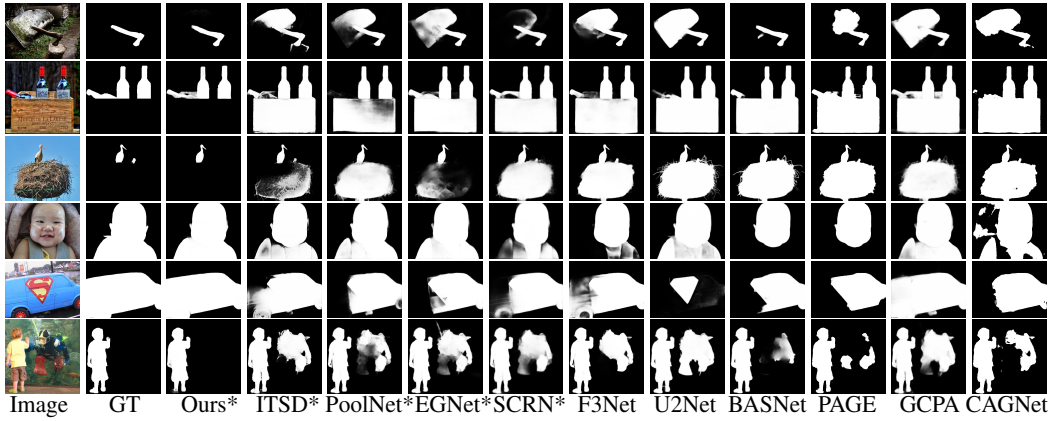


Figure 7: Visual comparisons between our method and 10 state-of-the-art networks. \* stands for models utilizing contour information. More comparisons are provided in the supplementary material.

outstanding results across all four metrics on most datasets. Besides, we demonstrate the standard PR and F-measure curves in Fig. 6. Our F-measure curves are flatter than all other models, which reveals that our results are closer to binary predictions and invariant to threshold changes.



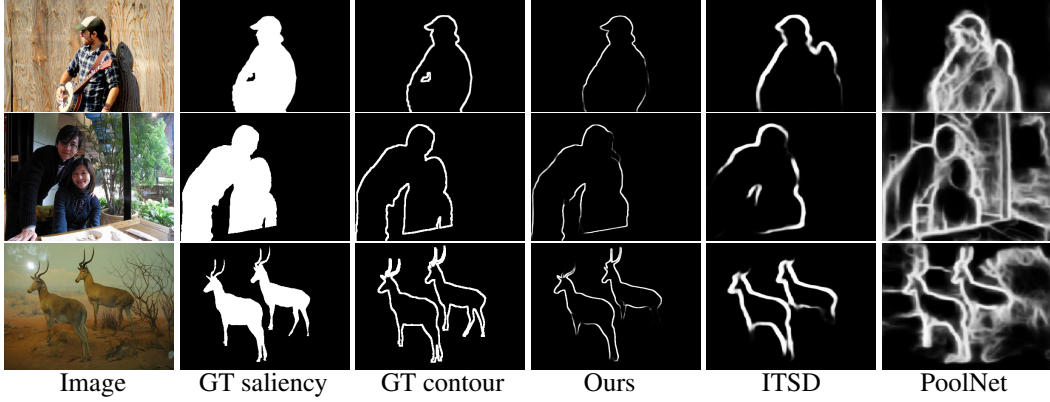


Figure 8: Visual comparison of contour predictions between our method, ITSD [56] and PoolNet [23]. Ground truth contours are obtained via erosion and dilation with kernel size of 5.

**Qualitative Evaluation.** Visual comparisons are listed in Fig. 7. Compare with other contour-based network results, our method yields better boundary predictions. As shown in the graph, our model can produce accurate and complete saliency maps with better edges.

**Visual Comparisons on Contour Predictions** Besides Fig. 1, we compare more on contour predictions of RCSB with ITSD [56] and PoolNet [23]. As illustrated in Fig. 8, RCSB can generate more complete and better contour predictions. This is due to the SFE module and the effectiveness of recursive mechanism where contour and saliency are blended multiple times.

#### 4.5 Ablation Studies

**Effectiveness of the Number of Recursions.** To investigate the effectiveness of recursion  $R$ , we gradually increase the recursion from 1 to 4 and measure  $F_\beta^*$ ,  $MAE$ ,  $E_\xi$ , and  $S_\alpha$  accordingly on DUTS-TE and ECSSD datasets. As shown in Table 2, when  $R$  equals 3, the model yields the best performance.

**Effectiveness of SFE Module and Different Loss Functions.** To study the importance of each loss function and SFE module, we conduct a series of controlled experiments on the DUTS-TE dataset, as listed in Table 3. First, we train the model by using BCE loss only, then include weighted IOU Loss [14], DCLoss, and CLoss step by step. Based on the results, when applying all four losses and with the SFE module, the model achieves the best performance.

Table 2: Ablation study for the effect of recursion number. When  $R=3$ , the best results are obtained.

	DUTS-TE				ECSSD			
	$F_\beta^* \uparrow$	$M \downarrow$	$E_\xi \uparrow$	$S_\alpha \uparrow$	$F_\beta^* \uparrow$	$M \downarrow$	$E_\xi \uparrow$	$S_\alpha \uparrow$
R=1	.882	.038	.899	.827	.943	.037	.917	.914
R=2	.886	.037	.901	.837	.944	.036	.918	.914
R=3	<b>.888</b>	<b>.036</b>	<b>.904</b>	<b>.878</b>	<b>.945</b>	<b>.037</b>	<b>.919</b>	<b>.916</b>
R=4	.885	.038	.900	.862	.943	.038	.916	.913

Table 3: Ablation study for different loss functions and presence of SFE module.

BCE	wIOU	DCLoss	CLoss	SFE	DUTS-TE			
					$F_\beta^* \uparrow$	$M \downarrow$	$E_\xi \uparrow$	$S_\alpha \uparrow$
✓					.863	.058	.862	.855
✓	✓				.875	.047	.881	.862
	✓	✓			.880	.043	.890	.867
	✓	✓	✓		.882	.040	.896	.870
	✓	✓	✓	✓	<b>.888</b>	<b>.036</b>	<b>.904</b>	<b>.878</b>

## 5 Conclusions

In this paper, we have introduced an efficient and accurate model using a recursive CNN together with a Contour-Saliency Blending (CSB) module. To further improve the model’s efficiency, a Stage-wise Feature Extraction (SFE) module is adopted. Furthermore, we divided the training objectives into accuracy and confidence, and proposed two loss functions to guide model convergence. The predicted salient objects achieved competitive state-of-the-art results on five benchmark datasets.

## References

- [1] R. Achanta, S. Hemami, F. Estrada, and S. Susstrunk. Frequency-tuned salient region detection. In *2009 IEEE Conference on Computer Vision and Pattern Recognition*, pages 1597–1604, 2009.
- [2] A. F. Agarap. Deep learning using rectified linear units (relu), 2018. cite arxiv:1803.08375Comment: 7 pages, 11 figures, 9 tables.
- [3] Q. Chen, T. Ge, Y. Xu, Z. Zhang, X. Yang, and K. Gai. Semantic human matting. In *Proceedings of the 26th ACM International Conference on Multimedia, MM '18*, page 618–626, New York, NY, USA, 2018. Association for Computing Machinery.
- [4] Z. Chen, Q. Xu, R. Cong, and Q. Huang. Global context-aware progressive aggregation network for salient object detection. *CoRR*, abs/2003.00651, 2020.
- [5] Z. Chen, H. Zhou, J. Lai, L. Yang, and X. Xie. Contour-aware loss: Boundary-aware learning for salient object segmentation. *IEEE Transactions on Image Processing*, 30:431–443, 2021.
- [6] M. Cheng, N. J. Mitra, X. Huang, P. H. S. Torr, and S. Hu. Global contrast based salient region detection. *IEEE Transactions on Pattern Analysis and Machine Intelligence*, 37(3):569–582, 2015.
- [7] D. Fan, M. Cheng, Y. Liu, T. Li, and A. Borji. Structure-measure: A new way to evaluate foreground maps. In *2017 IEEE International Conference on Computer Vision (ICCV)*, pages 4558–4567, Los Alamitos, CA, USA, oct 2017. IEEE Computer Society.
- [8] D.-P. Fan, C. Gong, Y. Cao, B. Ren, M.-M. Cheng, and A. Borji. Enhanced-alignment measure for binary foreground map evaluation. In *Proceedings of the Twenty-Seventh International Joint Conference on Artificial Intelligence, IJCAI-18*, pages 698–704. International Joint Conferences on Artificial Intelligence Organization, 7 2018.
- [9] H. Fang, S. Gupta, F. Iandola, R. Srivastava, L. Deng, P. Dollár, J. Gao, X. He, M. Mitchell, J. C. Platt, C. L. Zitnick, and G. Zweig. From captions to visual concepts and back, 2015.
- [10] M. Feng, H. Lu, and E. Ding. Attentive feedback network for boundary-aware salient object detection. In *2019 IEEE/CVF Conference on Computer Vision and Pattern Recognition (CVPR)*, pages 1623–1632, 2019.
- [11] K. He, X. Zhang, S. Ren, and J. Sun. Deep residual learning for image recognition. In *2016 IEEE Conference on Computer Vision and Pattern Recognition (CVPR)*, pages 770–778, 2016.
- [12] S. Ioffe and C. Szegedy. Batch normalization: Accelerating deep network training by reducing internal covariate shift. In F. Bach and D. Blei, editors, *Proceedings of the 32nd International Conference on Machine Learning*, volume 37 of *Proceedings of Machine Learning Research*, pages 448–456, Lille, France, 07–09 Jul 2015. PMLR.
- [13] B. Jiang, L. Zhang, H. Lu, C. Yang, and M. Yang. Saliency detection via absorbing markov chain. In *2013 IEEE International Conference on Computer Vision*, pages 1665–1672, 2013.
- [14] Q. H. Jun Wei, Shuhui Wang. F3net: Fusion, feedback and focus for salient object detection. In *AAAI Conference on Artificial Intelligence (AAAI)*, 2020.
- [15] M. Khalid, J. Baber, M. K. Kasi, M. Bakhtyar, V. Devi, and N. Sheikh. Empirical evaluation of activation functions in deep convolution neural network for facial expression recognition. In *2020 43rd International Conference on Telecommunications and Signal Processing (TSP)*, pages 204–207, 2020.
- [16] D. P. Kingma and J. Ba. Adam: A method for stochastic optimization, 2014. cite arxiv:1412.6980Comment: Published as a conference paper at the 3rd International Conference for Learning Representations, San Diego, 2015.
- [17] A. Krizhevsky, I. Sutskever, and G. E. Hinton. Imagenet classification with deep convolutional neural networks. *Commun. ACM*, 60(6):84–90, May 2017.
- [18] J. Kuen, Z. Wang, and G. Wang. Recurrent attentional networks for saliency detection. In *2016 IEEE Conference on Computer Vision and Pattern Recognition (CVPR)*, pages 3668–3677, 2016.
- [19] G. Li and Y. Yu. Visual saliency based on multiscale deep features. In *2015 IEEE Conference on Computer Vision and Pattern Recognition (CVPR)*, pages 5455–5463, Los Alamitos, CA, USA, jun 2015. IEEE Computer Society.
- [20] X. Li, F. Yang, H. Cheng, W. Liu, and D. Shen. Contour knowledge transfer for salient object detection. In *ECCV*, 2018.
- [21] Y. Li, X. Hou, C. Koch, J. M. Rehg, and A. L. Yuille. The secrets of salient object segmentation. In *2014 IEEE Conference on Computer Vision and Pattern Recognition*, pages 280–287, 2014.
- [22] T.-Y. Lin, P. Goyal, R. Girshick, K. He, and P. Dollár. Focal loss for dense object detection, 2018.
- [23] J.-J. Liu, Q. Hou, M.-M. Cheng, J. Feng, and J. Jiang. A simple pooling-based design for real-time salient object detection. In *IEEE CVPR*, 2019.

- [24] N. Liu, J. Han, and M. Yang. Picanet: Learning pixel-wise contextual attention for saliency detection. In *2018 IEEE/CVF Conference on Computer Vision and Pattern Recognition*, pages 3089–3098, 2018.
- [25] Z. Luo, A. Mishra, A. Achkar, J. Eichel, S. Li, and P. Jodoin. Non-local deep features for salient object detection. In *2017 IEEE Conference on Computer Vision and Pattern Recognition (CVPR)*, pages 6593–6601, 2017.
- [26] Z. Luo, A. Mishra, A. Achkar, J. Eichel, S. Li, and P. Jodoin. Non-local deep features for salient object detection. In *2017 IEEE Conference on Computer Vision and Pattern Recognition (CVPR)*, pages 6593–6601, 2017.
- [27] Y.-F. Ma, L. Lu, H.-J. Zhang, and M. Li. A user attention model for video summarization. In *Proceedings of the Tenth ACM International Conference on Multimedia*, MULTIMEDIA '02, page 533–542, New York, NY, USA, 2002. Association for Computing Machinery.
- [28] Ming Liang and Xiaolin Hu. Recurrent convolutional neural network for object recognition. In *2015 IEEE Conference on Computer Vision and Pattern Recognition (CVPR)*, pages 3367–3375, 2015.
- [29] S. Mohammadi, M. Noori, A. Bahri, S. G. Majelan, and M. Havaei. Cagnet: Content-aware guidance for salient object detection. *Pattern Recognition*, page 107303, 2020.
- [30] Y. Pang, X. Zhao, L. Zhang, and H. Lu. Multi-scale interactive network for salient object detection. June 2020.
- [31] A. Paszke, S. Gross, F. Massa, A. Lerer, J. Bradbury, G. Chanan, T. Killeen, Z. Lin, N. Gimelshein, L. Antiga, A. Desmaison, A. Kopf, E. Yang, Z. DeVito, M. Raison, A. Tejani, S. Chilamkurthy, B. Steiner, L. Fang, J. Bai, and S. Chintala. Pytorch: An imperative style, high-performance deep learning library. In H. Wallach, H. Larochelle, A. Beygelzimer, F. d'Alché-Buc, E. Fox, and R. Garnett, editors, *Advances in Neural Information Processing Systems 32*, pages 8024–8035. Curran Associates, Inc., 2019.
- [32] X. Qin, Z. Zhang, C. Huang, M. Dehghan, O. Zaiane, and M. Jagersand. U2-net: Going deeper with nested u-structure for salient object detection. volume 106, page 107404, 2020.
- [33] X. Qin, Z. Zhang, C. Huang, C. Gao, M. Dehghan, and M. Jagersand. Basnet: Boundary-aware salient object detection. In *2019 IEEE/CVF Conference on Computer Vision and Pattern Recognition (CVPR)*, pages 7471–7481, 2019.
- [34] O. Ronneberger, P. Fischer, and T. Brox. U-net: Convolutional networks for biomedical image segmentation. *CoRR*, abs/1505.04597, 2015.
- [35] C. Tang, X. Zhu, X. Liu, and P. Wang. Salient object detection via recurrently aggregating spatial attention weighted cross-level deep features. In *2019 IEEE International Conference on Multimedia and Expo (ICME)*, pages 1546–1551, 2019.
- [36] A. M. Treisman and G. Gelade. A feature-integration theory of attention. *Cognitive Psychology*, 12(1):97–136, 1980.
- [37] L. Wang, H. Lu, Y. Wang, M. Feng, D. Wang, B. Yin, and X. Ruan. Learning to detect salient objects with image-level supervision. In *2017 IEEE Conference on Computer Vision and Pattern Recognition (CVPR)*, pages 3796–3805, 2017.
- [38] L. Wang, L. Wang, H. Lu, P. Zhang, and X. Ruan. Salient object detection with recurrent fully convolutional networks. *IEEE Transactions on Pattern Analysis and Machine Intelligence*, 41(7):1734–1746, 2019.
- [39] W. Wang, S. Zhao, J. Shen, S. C. H. Hoi, and A. Borji. Salient object detection with pyramid attention and salient edges. In *2019 IEEE/CVF Conference on Computer Vision and Pattern Recognition (CVPR)*, pages 1448–1457, 2019.
- [40] Y. Wang, X. Zhao, X. Hu, Y. Li, and K. Huang. Focal boundary guided salient object detection. *IEEE Transactions on Image Processing*, 28(6):2813–2824, 2019.
- [41] Z. Wu, L. Su, and Q. Huang. Cascaded partial decoder for fast and accurate salient object detection, 2019.
- [42] Z. Wu, L. Su, and Q. Huang. Stacked cross refinement network for edge-aware salient object detection. In *2019 IEEE/CVF International Conference on Computer Vision (ICCV)*, pages 7263–7272, 2019.
- [43] K. Xu, J. Ba, R. Kiros, K. Cho, A. Courville, R. Salakhutdinov, R. Zemel, and Y. Bengio. Show, attend and tell: Neural image caption generation with visual attention, 2016.
- [44] Q. Yan, L. Xu, J. Shi, and J. Jia. Hierarchical saliency detection. In *2013 IEEE Conference on Computer Vision and Pattern Recognition*, pages 1155–1162, 2013.
- [45] C. Yang, L. Zhang, H. Lu, X. Ruan, and M. Yang. Saliency detection via graph-based manifold ranking. In *2013 IEEE Conference on Computer Vision and Pattern Recognition*, pages 3166–3173, 2013.
- [46] C. Yang, L. Zhang, H. Lu, X. Ruan, and M. Yang. Saliency detection via graph-based manifold ranking. In *2013 IEEE Conference on Computer Vision and Pattern Recognition*, pages 3166–3173, 2013.
- [47] A. R. Zamir, T.-L. Wu, L. Sun, W. Shen, J. Malik, and S. Savarese. Feedback networks, 2017.

- [48] L. Zhang, J. Dai, H. Lu, Y. He, and G. Wang. A bi-directional message passing model for salient object detection. In *2018 IEEE/CVF Conference on Computer Vision and Pattern Recognition*, pages 1741–1750, 2018.
- [49] L. Zhang, J. Dai, H. Lu, Y. He, and G. Wang. A bi-directional message passing model for salient object detection. In *2018 IEEE/CVF Conference on Computer Vision and Pattern Recognition*, pages 1741–1750, 2018.
- [50] P. Zhang, D. Wang, H. Lu, H. Wang, and X. Ruan. Amulet: Aggregating multi-level convolutional features for salient object detection, 2017.
- [51] X. Zhang, T. Wang, J. Qi, H. Lu, and G. Wang. Progressive attention guided recurrent network for salient object detection. In *2018 IEEE/CVF Conference on Computer Vision and Pattern Recognition*, pages 714–722, 2018.
- [52] X. Zhang, X. Zhou, M. Lin, and J. Sun. ShuffleNet: An Extremely Efficient Convolutional Neural Network for Mobile Devices. *arXiv e-prints*, page arXiv:1707.01083, jul 2017.
- [53] J.-X. Zhao, J. Liu, D.-P. Fan, Y. Cao, J. Yang, and M.-M. Cheng. Egnnet:edge guidance network for salient object detection, 2019.
- [54] R. Zhao, W. Ouyang, H. Li, and X. Wang. Saliency detection by multi-context deep learning. In *2015 IEEE Conference on Computer Vision and Pattern Recognition (CVPR)*, pages 1265–1274, 2015.
- [55] X. Zhao, Y. Pang, L. Zhang, H. Lu, and L. Zhang. Suppress and balance: A simple gated network for salient object detection. 2020.
- [56] H. Zhou, X. Xie, J.-H. Lai, Z. Chen, and L. Yang. Interactive two-stream decoder for accurate and fast saliency detection. In *IEEE/CVF Conference on Computer Vision and Pattern Recognition (CVPR)*, June 2020.
- [57] J. Zhu, J. Wu, Y. Xu, E. Chang, and Z. Tu. Unsupervised object class discovery via saliency-guided multiple class learning. *IEEE Transactions on Pattern Analysis and Machine Intelligence*, 37(4):862–875, 2015.